Development of Spark-Discharge System for Deposition of Metal Oxide Nanoparticles Having Uniform Distribution on Small Surface

F. Güngör[a,*], E. Güngör[b] and T. Güngör[b]

[a] *İzmir Science High School, 35040 İzmir, Türkiye*
[b] *Burdur Mehmet Akif Ersoy University, Energy Systems Engineering Department, 15030 Burdur, Türkiye*

Received: 07.10.2022 & Accepted: 13.02.2023

Doi: 10.12693/APhysPolA.143.284 *e-mail: fezagungor68@gmail.com

In the classical spark system, the fact that the distance between the electrodes is controlled separately with two separate micrometers can prevent the nanoparticles from properly coating the substrate surface. Therefore, in the present work, the classical system has been modified to eliminate this drawback. No study has been found in the literature with the simultaneous control of the distance between the electrodes. A microcontroller and electromechanical system were used in this modified spark discharge system. A shaft that has right and left teeth on it is driven by a microcontroller and moved by a stepper motor, providing simultaneous and equal control of the distance between the electrodes. In addition, with a second stepper motor, the circular movement of the substrate allowed the nanoparticles to accumulate around a center. The modified spark discharge system tested for undoped ZnO and Al-doped ZnO nanoparticles was synthesized with the Zn and Al metal electrode pairs such as Zn–Zn, Zn–Al, and Al–Al. The properties of thin films composed of nanoparticles were further studied by scanning electron microscopy, X-ray diffraction, and optical transmittance measurement. Based on the scanning electron microscopy analysis, it was observed that nanoparticles with smaller radii were obtained in a circular area in the center of the substrate, and these nanoparticles covered the substrate surface more smoothly and homogeneously. The average nanoparticle diameters for Zn–Zn electrodes were calculated as 94 nm and 42 nm for the classical spark discharge system and the modified spark discharge system, respectively. When Al–Zn electrodes were used, it was observed that the average size of the nanoparticles was 57 nm and that they were distributed very smoothly and homogeneously on the substrate surface. In addition, a decrease in optical transmittance values was observed due to decreasing mean radius values and uniformly dispersed nanoparticles.

topics: Al:ZnO nanoparticles, metal oxide nanoparticles, spark discharge method, optical transmittance of oxides

1. Introduction

Nanotechnology is extensively employed in various application areas, including the semiconductors industry and medicine. Transition metal oxides have acquired much attention owing to their wide potential technological applications [1–3]. Considering these different usage areas, nanoparticles (NPs) are produced with different production techniques. Several synthesis techniques are available for the production of NPs, such as sol–gel, precipitation, thermal oxidation, microwave-assisted solvothermal method [4–6], direct current (DC) magnetron sputtering [7], radio frequency (rf) magnetron sputtering [8], pulsed laser deposition (PLD) [9], vacuum arc plasma evaporation (VAPE) [10], and spark discharge technique [11, 12]. The spark discharge technique, which was first used by Schwyn in 1988 [11], is one of the simple, compact, and versatile methods to produce NPs from different types of materials. In addition, the synthesis can be performed at atmospheric pressure or in a dielectric liquid medium [13, 14], which is quite economical in comparison to vacuum methods and has the potential of being scaled up. This method was used for depositing ZnO NPs [12], Co-doped ZnO NPs, and Cu-doped ZnO NPs using high-purity Zn, Co, and Cu metals [15, 16]. In the classical spark discharge (CSD) technique, which is one of the plasma-based material preparation techniques, first, a high voltage difference is applied between two metal electrodes with sufficient distance between them. As the spark formed in this way evaporates the electrode tips, the metal particles released combine with the oxygen in the atmosphere and are deposited on the substrate surface as metal oxide nanoparticles. In the CSD system, micrometers are used to control the distance between two metal electrodes

positioned horizontally or vertically. To keep the distance between two electrodes constant during nanoparticle deposition, it is necessary to move the two-micrometer arms separately in a controlled manner. In this system, if the movement cannot be achieved on the same axis and at equal intervals, NPs cannot be properly concentrically placed in the target area on the substrate surface. NPs cannot be deposited on the surface uniformly, and the desired efficiency cannot be obtained from the structural, optical, and electrical properties of the film formed. For example, an NPs-coated surface is obtained that does not transmit enough light or has a very high resistivity other than the intended use of the produced material. Whereas, while one of the electrodes is fixed in the experiments carried out in the dielectric liquid, the motion control of the other electrode can be provided with the help of a servo motor. For such systems, the motion control of the two electrodes may not be important because the nanoparticles formed by spark discharge are suspended in the dielectric liquid [13, 14].

In this study, a microcontroller and stepper motors were used, instead of micrometers, to control the distance between the electrodes by modifying the CSD system. Hence, metal electrodes can be controlled using a microcontroller, they are brought close to each other on the co-axis and at an equal distance by employing a stepper motor, and circular movement of the substrate can be achieved with the secondary stepper motor. Thin films consisting of NPs produced using this new modified spark discharge (MSD) system were examined structurally and optically, and the results were compared with the results of the films produced with the current CSD, which was referenced.

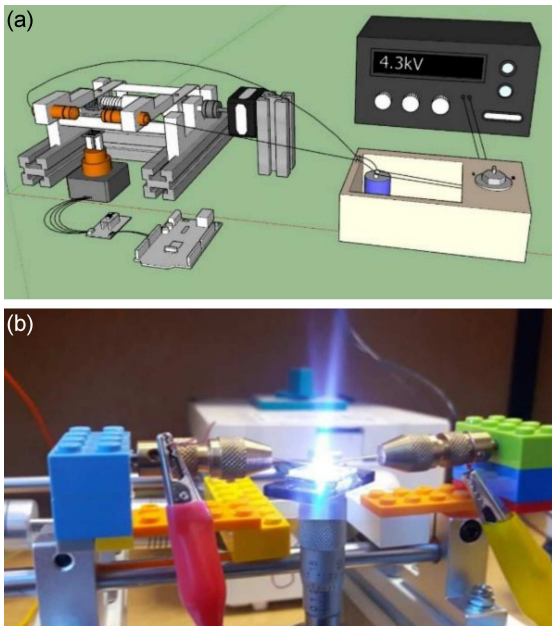

Fig. 1. Illustration of MSD system (a) and a photograph of the spark discharge moment (b).

TABLE I

Sample parameters for 4.3 kV spark-discharge voltage; D is the crystallite size obtained from (1).

Electrode pairs	Thickness [nm]	D [nm]	NP's size [nm]	Atomic Percentage [%]		
				Zn	Al	O
Zn–Zn	145	70	42	21	–	59
Al–Zn	468	65	57	48	0.52	61
Al–Al	138	60	*160, **183	–	0.87	56

*Average edge lengths of cubic nanoparticles

**Average spherical nanoparticles diameter

2. Materials and methods

The system used to obtain nanoparticles by CSD system (see [15, 16] for details) consists of a regulated DC high voltage source, a capacitor used to store electrostatic energy, and high-purity metal electrodes (Fig. 1). In the classical method, the distance between the electrodes is controlled manually with the help of two micrometers, trying to keep it constant during the deposition of the nanoparticles. For the CSD system, the microscope glass used as a substrate is kept constant during the nanoparticle deposition process. However, the substrate can be moved circularly during the deposition to ensure homogeneous distribution of nanoparticles in the MSD system. Here, the rotation speed of the substrate is controlled by a microcontroller (Arduino Uno) and a stepper motor driver unit. To precisely control the distance between the metal electrodes, an electro–mechanical unit was designed. For the mechanical part, half of one shaft is threaded right, and the other half is left threaded with metric 8 (M8X1.25). For the electronic part, this unit is combined with a second stepper motor driver unit with a microcontroller. The second stepper motor completes one revolution with different steps (up to 2, 4, 8, 16, 32,... 25600 steps) optionally as multiples of 2. The mechanical system carrying the metal electrodes is supported by 2 ball bearings and chrome shafts. Thus, the distance between the electrodes during spark discharge can be controlled in the order of approximately 0.05 μm. With this system, the electrostatic energy (1.85 J), stored in the capacitor (0.2 μF/5 kV) under a voltage difference of 4.3 kV, was discharged (Fig. 1b) between the high-purity Al and Zn (>99.95%) electrodes by precisely controlling the metal electrodes.

The microscope glasses ($10 \times 10 \times 1$ mm^3) were used as the substrate, which was sonically cleaned in distilled water, ethanol, and acetone, and then dried. Zn, Al, and Zn–Al mixture nanoparticles were obtained by spark discharge (200 times with a speed of about 3 s/spark). Parameters of the samples are given in Table I.

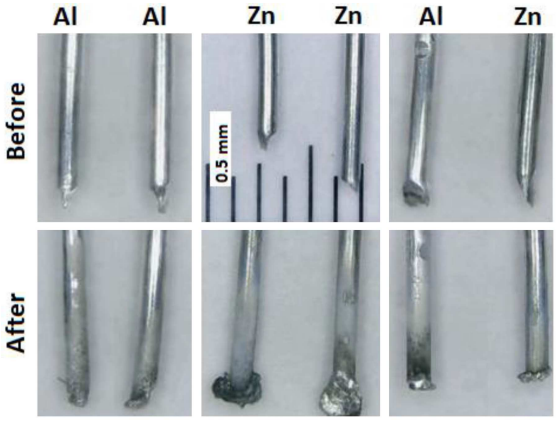

Fig. 2. Photographs of metal electrodes (Al–Al, Zn–Zn, and Al–Zn) before and after spark discharge for the MSD system.

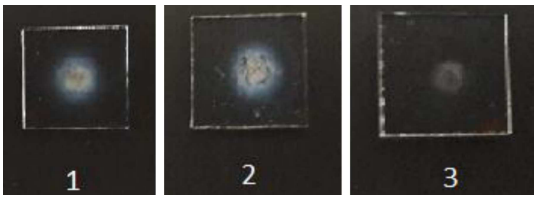

Fig. 3. Photographs of thin film samples formed from nanoparticles obtained by using Al–Zn (no. 1), Zn–Zn (no. 2), and Al–Al (no. 3) electrode pairs with the MSD system.

Experimental optical transmittance spectra of nanoparticles were obtained at room temperature using a spectrophotometer (Seeman 3000) with a CCD (Charge Coupled Device) detector in the wavelength range of 300–1100 nm. The phase analysis has been carried out using an X-ray diffraction (XRD) meter (Bruker AXS D8 Advance Model, Cu $K_{\alpha 1}$ ($\lambda = 1.5405$ Å)). A scanning electron microscope (SEM, FEI Quanta FEG 250) was used to examine the surface properties, and energy dispersive spectroscopy (EDS) analyses were used to determine atomic concentrations.

3. Results and discussion

Photographs of Al and Zn metal electrode before and after spark discharge are shown in Fig. 2. In addition, photographs of thin film samples formed from nanoparticles obtained by using Al–Zn (no. 1), Zn–Zn (no. 2), and Al–Al (no. 3) electrode pairs are depicted in Fig. 3.

3.1. Structural properties

XRD patterns of Al-based oxide (Al_2O_3) obtained by using Al–Al electrode pairs are shown in Fig. 4, of undoped ZnO obtained by using Zn–Zn electrode pairs — in Fig. 5, and of Al-doped ZnO obtained by using Zn–Al electrode pairs — in Fig. 6. Reference databases, such as PDF 00-002-1422 with JCPDS 35-0121 for Al-related phases and JCPDS 36-1451 for ZnO-related phases, were used for detailed analysis of XRD patterns. The results indicate that the (100) peak of the hexagonal wurtzite structure of ZnO is observed for Zn–Zn electrodes. In addition, the diffraction peak at around 32.103° associated with (200) for Al–Al electrodes indicates Al_2O_3 is in monoclinic structure and θ-phase. This phase is consistent with the value found in the literature [17]. When XRD databases were examined, a dominant (relatively intense) reflection peak was found with angular positions of 32.173° for ZnO and 32.054° for Al_2O_3. Considering the information for Al- and Zn-related phases in the database,

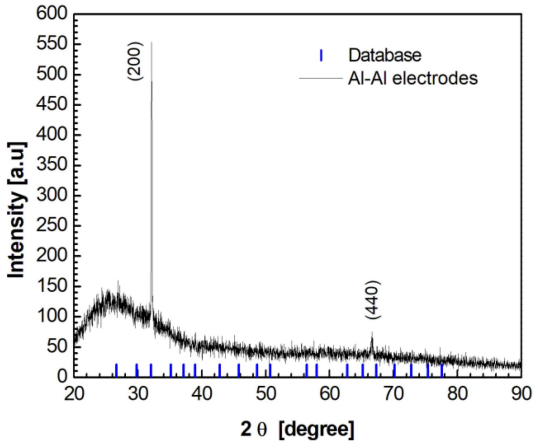

Fig. 4. XRD patterns of Al-based oxide (θ-Al_2O_3) obtained by using Al–Al (black line) electrode pairs with MSD system. The reference diffraction peaks obtained from PDF 00-002-1422 are indicated by blue color ticks (|).

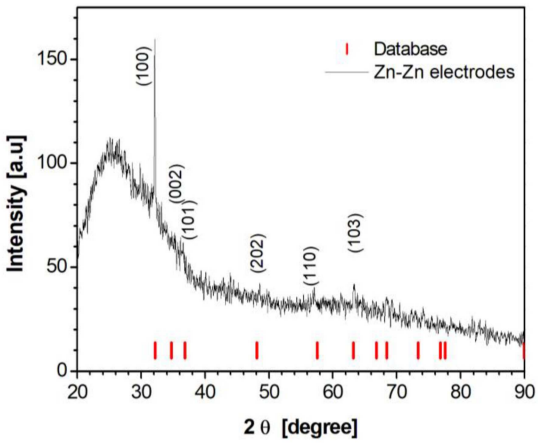

Fig. 5. XRD patterns of undoped ZnO obtained by using Zn–Zn (black line) electrode pairs with MSD system. The reference diffraction peaks (JCPDS 36-1451) are indicated by red color ticks (|).

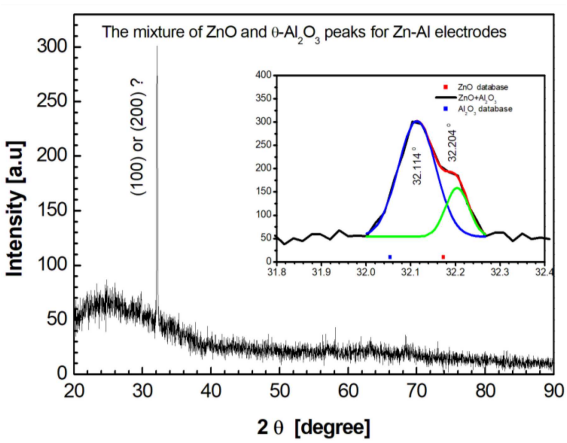

Fig. 6. XRD patterns of Al-doped ZnO obtained by using Zn–Al electrode pairs with MSD system. Detailed peak analysis is depicted in the inset in the figure. Nested diffraction peaks are indicated by blue and green lines.

the difference between these intense peaks is 0.119°. This value was used as a reference for comparison with the results of the experiments in this study. It was observed that the XRD pattern of the Al:ZnO film obtained by using Al–Zn electrodes had nested peaks in the 32° centered region. This can be explained by the fact that the atomic radius of Al^{3+} (0.53 pm) is smaller than the atomic radius of Zn^{2+} (74 pm). Therefore, to analyze these peaks, a Gaussian function with two peaks was fitted to the experimental XRD pattern. The reflection peak of the ZnO phase was found at 32.204°, and the reflection peak of Al_2O_3 phase was found at 32.114° (inset in Fig. 6). The difference between the examined reflection peaks was calculated as 0.110°. This difference is very close to the reference value. As a result, it was determined that the thin film samples formed by ZnO, Al_2O_3, and Al:ZnO NPs were obtained for Zn–Zn, Al–Al, and Zn–Al electrodes, respectively. The crystallite size (D) was calculated from the Debye–Scherrer equation [18] given by

$$D = \frac{K\,\lambda}{\beta\cos(\theta)}, \tag{1}$$

where β is the intensity at FWHM, θ is the diffraction angle, and K and X-ray wavelength λ constants are 0.9 and 0.15406 nm, respectively. Using the full width at half maximum (FWHM) of the maximum peaks provided from the XRD patterns, the crystallite sizes of the nanoparticles obtained using the Zn–Zn, Zn–Al, and Al–Al electrodes were calculated to be, respectively, 70 nm, 65 nm, and 60 nm (Table I).

The SEM analysis was carried out at the center of the spark-affected area with high magnification. Figure 7 shows the SEM images of ZnO NPs deposited using Zn–Zn electrodes for CSD and MCD systems.

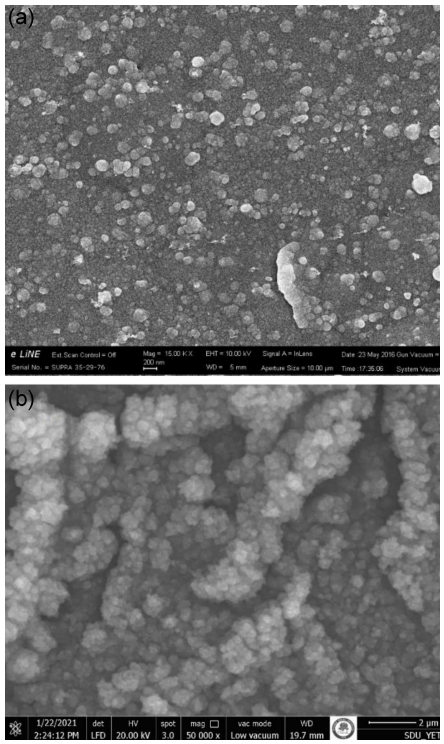

Fig. 7. SEM images for the samples obtained with Zn–Zn electrodes for CSD system [15] (a) and MSD system (b).

When examining the particles, it was found that the axial movement control of electrodes affects the shape of the nanoparticles as well as the NP's size distribution. The size distributions of nanoparticles obtained by using Zn–Zn electrodes in the CSD system are shown in Fig. 8a and b. The average nanoparticle diameters were calculated as 42 nm and 94 nm for the MSD system and the CSD system, respectively. When Al–Zn electrodes were used, it was observed that the average size of the nanoparticles was 57 nm, and they were distributed very smoothly and homogeneously on the substrate surface (Fig. 9a). This uniform distribution can be explained by the presence of Al atoms located between the Zn atoms. However, it was observed that the nanoparticles did not properly cover the substrate surface when Al–Al electrodes were used. Spherical nanoparticles and cubic nanoparticles were observed. The average size of the spherical nanoparticles was calculated as 183 nm, and the edge length of the cubic nanoparticles was calculated as 160 nm. The distance between these particles is also quite large (Fig. 9b).

The chemical composition of the nanodots was measured using EDX. It was found that oxygen was dominant compared to Zn and Al ions. The atomic percentage of Zn and oxygen were observed as 21% and 59% for the pair of Zn–Zn electrodes, respectively. However, the atomic percentage of Al and oxygen were observed as 0.87% and 56% for the pair of Al–Al electrodes. The atomic percentage of Zn,

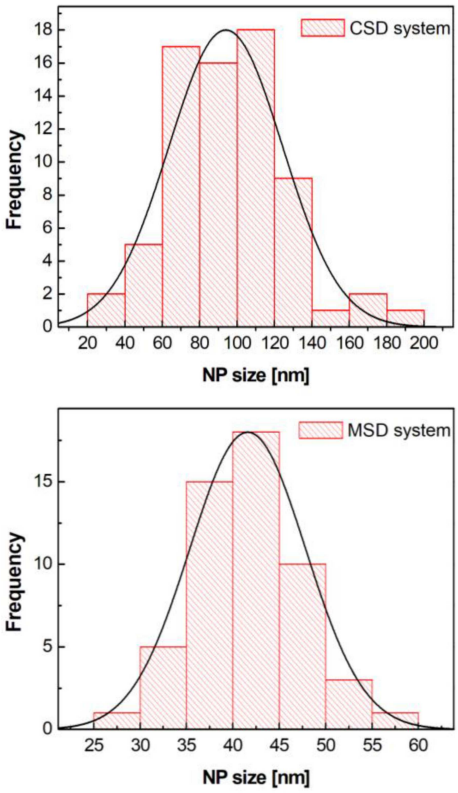

Fig. 8. Size distribution of nanoparticles for CSD system (a) and MSD system (b) using Zn–Zn electrode pairs.

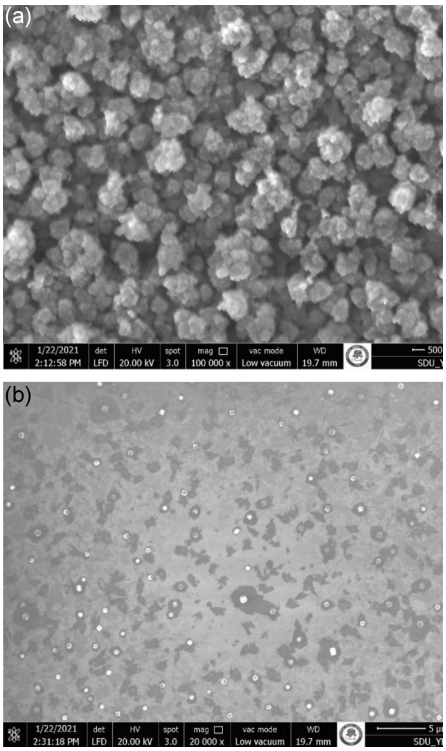

Fig. 9. SEM images for the samples obtained with MSD system Zn–Al electrodes (a) and Al–Al electrodes (b).

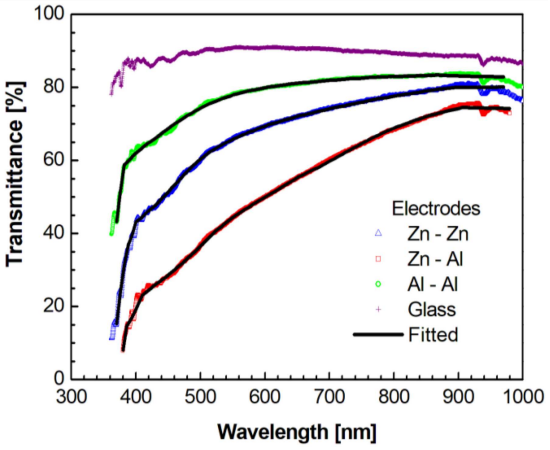

Fig. 10. Experimental and theoretical optical transmission spectra are shown by symbols (□, ◯, △) and black lines, respectively. The optical transmittance spectrum of microscope glass used as a substrate is shown by symbol (+).

Al, and oxygen were found as about 48%, 0.52%, and 61% for pairs of Zn–Al electrodes. It has been observed that when aluminum is desired to be deposited on the substrate together with zinc, zinc covers the surface more predominantly. This situation is in harmony with the dominance of the ZnO phase in the XRD spectrum.

3.2. Optical properties

Considering that the substrate surface coated with metal nanoparticles can be accepted in the form of thin film, the wavelength-dependent relative optical transmittance of thin films at room temperature was measured (Fig. 10). The thickness of the thin films was determined by one of the iterative methods based on the pointwise unconstrained minimization algorithm (PUMA) [19]. This algorithm generates a theoretical optical transmittance spectrum that matches the experimental optical transmittance spectrum by scanning user-specified solution spaces for film thickness and optical constants. In this way, it gives the film thickness information. Thicknesses of thin films coated with Al–Al, Zn–Zn, and Al–Zn electrodes were determined as 138 nm, 145 nm, and 468 nm, respectively. There is excellent agreement between the experimental spectra and theoretical spectra (Fig. 10).

When the microscope glass used as the substrate is taken as a reference, it was observed that the optical transmittance of the thin film sample formed by Al_2O_3 NPs using Al–Al electrodes decreased. This decrease was also observed in thin film samples formed by ZnO NPs and Al_2O_3 and ZnO NPs, respectively (Fig. 10). According to the results of

SEM analysis, when Al–Al electrodes are used, although the average particle size in the sample film is 160 nm, the distance between nanoparticles is approximately in the range of 1–2 μm. However, optical transmittance measurements are in the wavelength range of 0.3–1 μm. Accordingly, since the wavelength of the light used for optical transmittance measurements is smaller than the distance between nanoparticles, the incident light reached the detector in the spectrophotometer without scattering. Therefore, this sample was observed as having high optical transmittance. However, for both Zn–Zn electrodes and Al–Al electrodes used, the average size of NPs formed is in the order of 50 nm. The decrease in NP diameter causes scattering of the light passing through the uniformly distributed nanoparticles deposited region, which leads to a decrease in the optical transmittance.

4. Conclusions

In this study, an electro–mechanical unit that provides a uniform coating of nanoparticles on the substrate surface with the innovations made to the CSD system has been designed and tested. As the first modification, instead of two separate micrometer arms, a specially designed shaft was used to control the distance between the electrodes. This shaft can complete one full revolution in 25600 steps with the help of a microcontroller and step motor. Thus, the distance between the electrodes during spark discharge can be controlled in the order of approximately 0.05 μm. The second modification is the circular movement of the substrate using a second stepper motor. It has been observed that nanoparticles cover the substrate surface more smoothly and in smaller sizes in a circular region. With the help of this circular motion, aggregation of nanoparticles that appeared in successive sparks was also prevented. ZnO nanoparticles obtained with Zn electrodes were used to compare the nanoparticle size distributions obtained in the CSD and MSD systems. It was observed that the modified system was more effective and successful. It has been noticed that the size distribution of nanoparticles affects optical transmittance. As a result, uniform thin films coated with nanoparticles with smaller diameters can be obtained by using similar or different electrode pairs with the modified spark discharge system. Larger areas can be covered with nanoparticles using a stepper-motor-controlled mechanical unit added to the system that provides axial or planar motion. In addition, ion seeding can be done on thin films prepared previously with the same system or with different deposition systems. In this way, it can be used in various technological applications, considering changes in the physical and structural properties of the materials prepared with the MSD system.

Acknowledgments

This study was supported by the Scientific Research Unit of Burdur Mehmet Akif Ersoy University with the project number 0253-MP-14.

References

[1] D. Li, J. Hu, R. Wu, J.G. Lu, *Nanotechnology* **21**, 485502 (2010).

[2] Y. Xu, D. Chen, X. Jiao, *J. Phys. Chem. B* **109**, 13561 (2005).

[3] J. Huang, S.R. Wang, Y. Q. Zhao, X.Y. Wang, S.P. Wang, S.H. Wu, S.M. Zhang, W.P. Huang, *Catal. Commun.* **7**, 1029 (2006).

[4] V. Usha, S. Kalyanaraman, R. Thangave, R. Vettumperumal, *Superlattices Microstruct.* **86**, 203 (2015).

[5] M. Sahooli, S. Sabbaghi, R. Saboori, *Mater. Lett.* **81**, 169 (2012).

[6] S. G. Rejith, C. Krishnan, *Mater. Lett.* **106**, 87 (2013).

[7] P. Asanithi, S. Chaiyakun, P. Limsuwan, *J. Nanomater.* **2012**, 963609 (2012).

[8] Y. Xiong, H. Wu, Y. Guo, Y. Sun, D. Yang, D. Da, *Thin Solid Film.* **375**, 300 (2000).

[9] A.O. Dikovska, M.T. Alexandrov, G.B. Atanasova, N.T. Tsankov, P.K. Stefanov, *Appl. Phys. A* **113**, 83 (2013).

[10] N. Matsumoto, H. Kinoshita, N. Ohmae, *Diamond Relat. Mater.* **109**, 108048 (2020).

[11] S. Schwyn, E. Garwin, A. Schmidtott, *J. Aerosol. Sci.* **19**, 639 (1988).

[12] T. Kumpika, W. Thongsuwan, P. Singjai, *Thin Solid Films* **516**, 5640 (2008).

[13] K.H. Tseng, C.T. Yeh, M.Y. Chung, Y.S. Lin, N. Qui, *Sci. Rep.* **11**, 20457 (2021).

[14] K.H. Tseng, W.J. Lin, M.Y. Chung, D.C. Tien, L. Stobinski, *J. Clust. Sci.* **33**, 2069 (2022).

[15] E. Gungor, T. Gungor, D. Caliskan, E. Ozbay, *Acta Phys. Pol. A* **131**, 500 (2017).

[16] T. Gungor, E. Gungor, D. Caliskan, E. Ozbay, *Acta Phys. Pol. A* **135**, 857 (2019).

[17] D. Manyasree, P. Kiranmayi, R.V.S.S.N. Ravi Kumar, *Int. J. Pharm. Pharm. Sci.* **10**, 32 (2018).

[18] B.D. Cullity, *The Elements of X-Ray Diffraction*, 2nd ed., Addison-Wesley, Reading (MA) 1978.

[19] E.G. Birgin, I. Chambouleyron, J.M. Martinez, *J. Comput. Phys.* **151**, 862 (1999).